Extending the Phase Gradient Autofocus Algorithm for Low-Altitude Stripmap Mode SAR

Douglas G. Thompson, James S. Bates, David V. Arnold
Brigham Young University
459 CB, Provo, UT 84602
voice: 801-378-4884, FAX: 801-378-6586, e-mail: thompsod@ee.byu.edu

Abstract— The Phase Gradient Autofocus (PGA) algorithm has been widely used in Spotlight Synthetic Aperture Radar (SAR) to remove motion-induced blurs in the images. The PGA algorithm has been proven to be a superior autofocus method. This algorithm is extended for application to low-altitude stripmap mode SAR. PGA assumes a narrow beam, which is valid for most SAR systems. However, lower altitude SARs have large range dependencies that cannot be ignored. A new phase estimator for PGA is introduced and extended to allow range dependence. Three SAR images with different characteristics are used in simulations comparing the new estimator to the widely used maximum likelihood approach and in demonstrating the range-dependent PGA algorithm. The PGA algorithm is also extended to stripmap mode SAR data through a new compression method.

INTRODUCTION AND BACKGROUND

Full focusing of SAR images requires some type of autofocus routine. The Phase Gradient Autofocus (PGA) algorithm has proven to be a superior method for higher order autofocus because it does not assume a model for the phase error. The standard PGA model assumes a small beamwidth in range, which results in a phase error constant in the range direction. Most satellites and other high altitude systems fit this model. However, a low-altitude SAR like YSAR [1] will have range-dependent phase errors. The PGA algorithm is well-developed only for spotlight mode SAR data. In this paper we extend the algorithm by introducing range dependencies in the phase error and by applying the algorithm to stripmap mode data.

There are four main steps in the PGA algorithm. The four steps are center shifting, windowing, phase estimation and iteration. These steps are described in detail in [2, 3, 4]. A few different methods have been proposed for the phase estimation step, with different criteria for optimality. The original algorithm used linear unbiased minimum variance [2]. The same authors later proposed a method using a maximum likelihood (ML) estimator [3]. This paper proposes a new phase estimation technique which allows extension to a range-dependent algorithm. The Phase Weighted Estimation PGA (PWE-PGA) proposed here differs from earlier algorithms only in the phase estimation step. This phase estimator can be used equally well in stripmap or spotlight mode data, and in range dependent or non-range dependent versions. The stripmap mode algorithm proposed here differs from other versions in a few ways, primarily in a preprocessing step and in the circular shifting step.

The following section describes the cause of the range dependencies in low-altitude SAR data. The next section describes the proposed phase estimator and the extension to the range dependent version and presents results of some simulations using this method on spotlight SAR data. The next section discusses the stripmap mode PGA algorithm. Conclusions and future work are discussed in the final section.

RANGE-DEPENDENT PGA

The traditional PGA algorithm described above assumes that the phase error is constant with range and estimates the error as a function of azimuth position. A low-altitude SAR system with highly varying incidence angles will exhibit range-dependent effects in the phase errors. This section describes the cause of some of these range dependencies.

Assume the instrument platform is flying with constant velocity in the direction of increasing z, with the nominal trajectory following $x = y = 0$, as shown in Fig. 1. Then the phase error due to the trajectory errors in the x and y directions can be written as

$$\phi(t,\theta) = \frac{4\pi}{\lambda}(-x(t)\sin(\theta) + y(t)\cos(\theta)), \tag{1}$$

where θ is the incidence angle. The data is stored by range bin instead of incidence angle, so we write the incidence angle for the kth range bin as

$$\theta_k = \cos^{-1}\left(\frac{H}{R_0 + kR}\right). \tag{2}$$

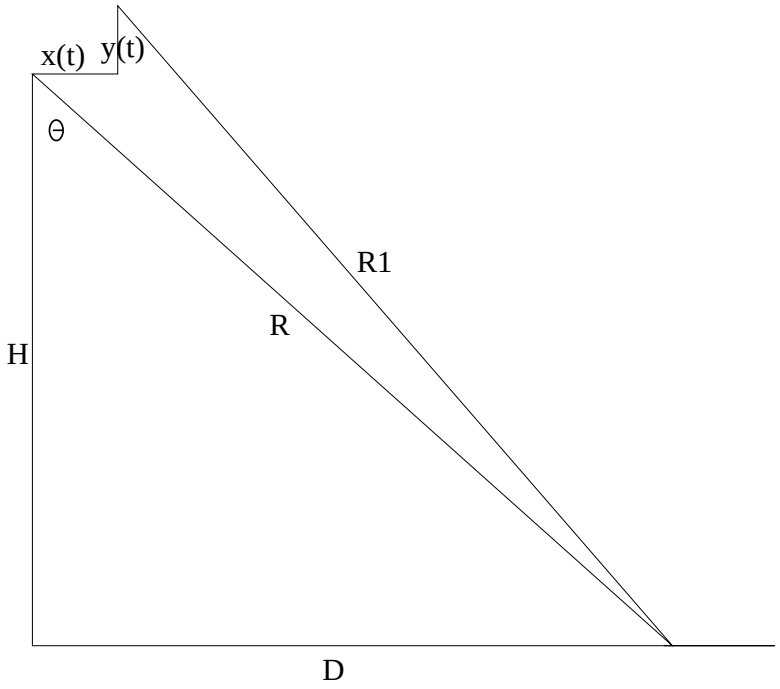

Figure 1: Transverse Motion Geometry

Here H represents the height of the instrument above the topography, R_0 is the range to the zeroth sample, and R is the range bin size. Now we have two parameters of phase error to estimate for each azimuth position, $\hat{\phi}_x = -\frac{4\pi}{\lambda}x(t)$ and $\hat{\phi}_y = \frac{4\pi}{\lambda}y(t)$. There is still a large amount of redundancy in the data, so one should be able to effectively estimate these two parameters by adding some kind of range-dependent weighting in the PGA phase estimator. One possibility for the range-dependent weighting is developed in the following section.

PHASE WEIGHTED ESTIMATION

To apply PGA, the gradient of the phase error must be found. The maximum likelihood method is known to be optimal and robust; thus, a first approach would be to apply this method to the range-dependent problem. However, we are not aware of a closed form for the phase estimate in this case. We thus introduce a new algorithm to estimate the phase gradient which allows a simple closed form for a range-dependent version. The phase noise of a sample depends inversely on the magnitude. Thus, our new method weights the phase measurements by the magnitude of the corresponding pixel. This method is weighted least squares optimal.

Let g_{kn} denote the image in the range-compressed domain, with k indicating the range bin and n the azimuth bin. Then the estimated phase gradient, denoted $\hat{\phi}_n$, is

$$\hat{\phi}_n = \frac{\sum_{k=0}^{M-1}\left(|(g_{kn}g^*_{k(n-1)})|\angle(g_{kn}g^*_{k(n-1)})\right)}{\sum_{k=0}^{M-1}|(g_{kn}g^*_{k(n-1)})|}. \tag{3}$$

We now extend this algorithm to the range dependent form. Any algorithm using a weighting of the phase values in the form of Eq. 3 can easily by extended to this form without changing the phase weighting. We simply add range weighting and write a vector of equations indexed by range bin k as

$$\hat{\phi}_{xn}\sin(\theta_k) + \hat{\phi}_{yn}\cos(\theta_k) = \frac{|g_{kn}g^*_{k(n-1)}|}{\text{mean}(|g_{kn}g^*_{k(n-1)}|)}\angle(g_{kn}g^*_{k(n-1)}). \tag{4}$$

This equation is separated into vectors and matrices and written as

$$\mathbf{A}\hat{\phi}_{\mathbf{n}} = \tilde{\phi_{\mathbf{kn}}} \tag{5}$$

where $\mathbf{A}$ is the Mx2 matrix made up of the sine values in the first column and the cosine values in the second, $\hat{\phi}_{\mathbf{n}}$ is the 2x1 vector of phase estimates, and $\tilde{\phi_{\mathbf{kn}}}$ is the Mx1 vector of weighted image phase gradients. This equation is solved using the pseudoinverse of $\mathbf{A}$ to obtain the range-dependent phase gradient estimate. This gradient is then integrated and applied in the same way as in the original PGA algorithm. This algorithm can be derived using standard weighted least squares methods and is optimum in that sense [5].

The new PWE-PGA algorithm was tested using synthetic phase errors on three different SAR images. The first is a desert region with no significant scatterers. The second is a mountain region with some prominent scatterers. The third is an urban region with many scatterers of all types. Range dependent and non-range dependent phase errors were applied to each image, and the blurred images were corrected using the original ML-PGA algorithm and using the new Phase Weighted Estimation PGA. For the non-range dependent tests, the ML-PGA results are compared with the PWE-PGA. In each case, the PWE-PGA converges much more slowly than ML-PGA but has a smaller error after many iterations.

In all of these tests, the phase error is estimated and removed very accurately such that the restored image is nearly indistinguishable from the original. For some range dependent tests, the individual parameters ϕ_x and ϕ_y have a relatively large error, but the combined phase error estimate at any given range is accurate. This is because of the non-uniqueness of the pseudoinverse. Different linear biases in ϕ_x and ϕ_y can also cause a range-dependent shift, distorting the image slightly.

Actual and estimated phase errors for the three images for non-range dependent errors are shown in Figs. 2, 3, 4. The standard deviation is plotted as a function of iteration in Figs. 5, 6, 7 for the same tests. Results of the range dependent tests for the urban image only are shown in Figs. 8-12. These figures show the phase error comparison in ϕ_x and ϕ_y and total phase error at near, mid, and far ranges, respectively.

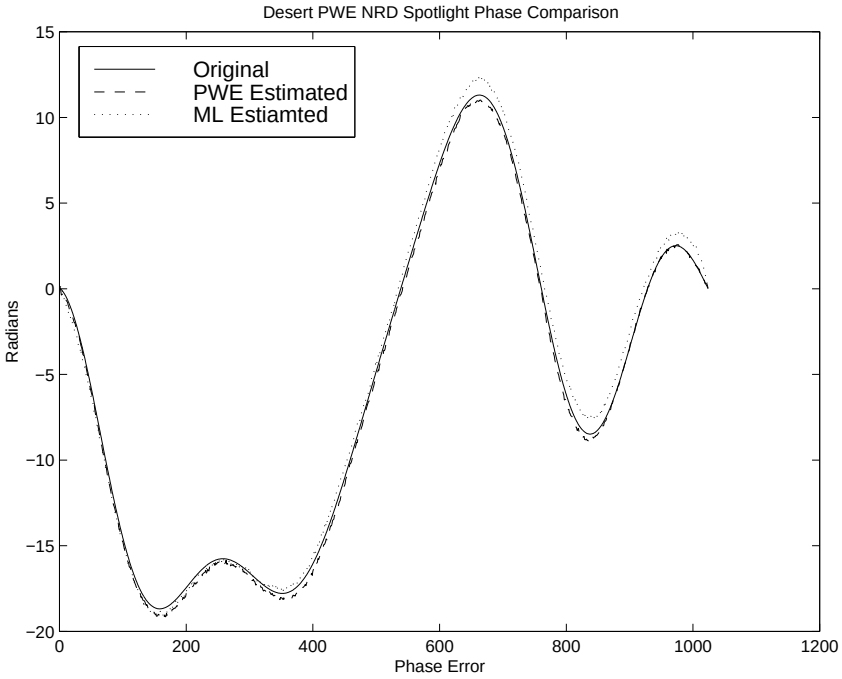

Figure 2: Phase error comparison, PWE-PGA vs. ML-PGA for non-range dependent spotlight desert image.

STRIPMAP MODE PGA

The PGA algorithm as discussed above does not apply to stripmap mode SAR data. The stripmap mode SAR uses chirp correlation instead of Fourier transformation to transform from range-compressed to fully-compressed data. Also, each pixel in a spotlight image contains the phase history for all of the data, while the stripmap phase history is limited by the azimuth

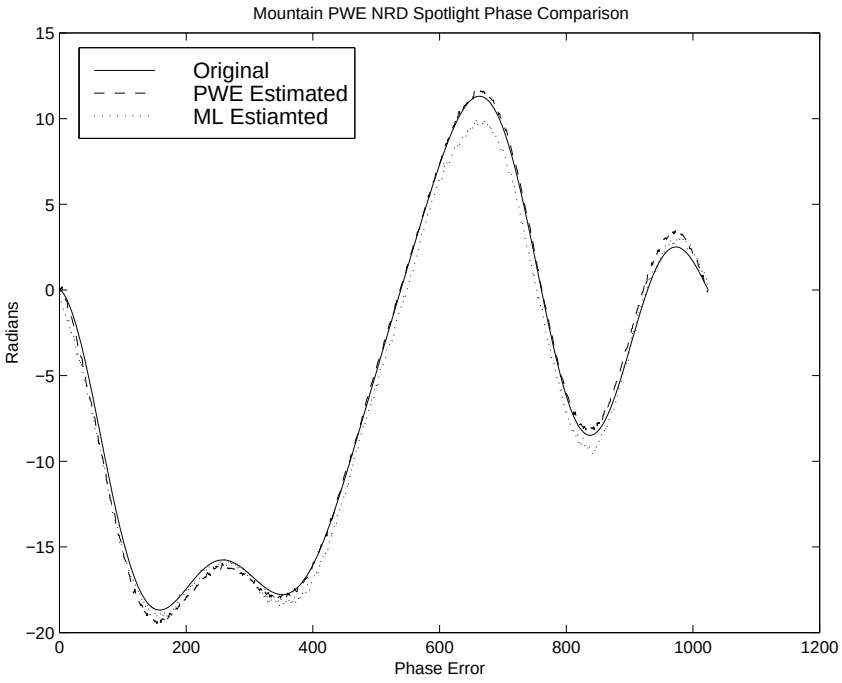

Figure 3: Phase error comparison,PWE-PGA vs. ML-PGA for non-range dependent spotlight mountain image.

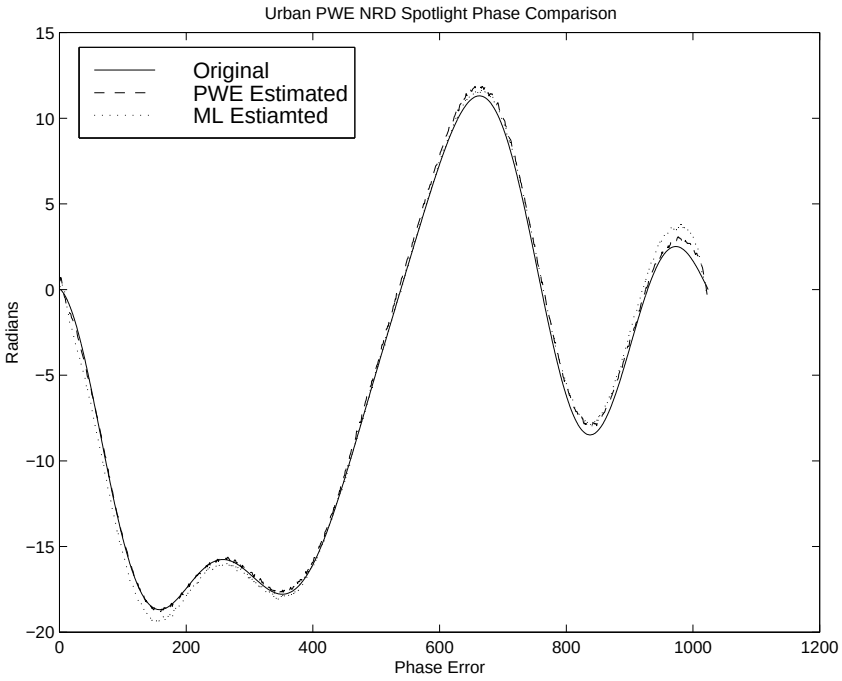

Figure 4: Phase error comparison, PWE-PGA vs. ML-PGA for non-range dependent spotlight urban image.

beamwidth. Stripmap to spotlight data formatters have been proposed [6, 7], but these algorithms make the narrow-beam assumption and cannot easily be extended to the range-dependent case. We introduce an alternative compression algorithm to be used for phase error estimation. This new method will be called Stripmap Spotlight Compression (SSC) because of

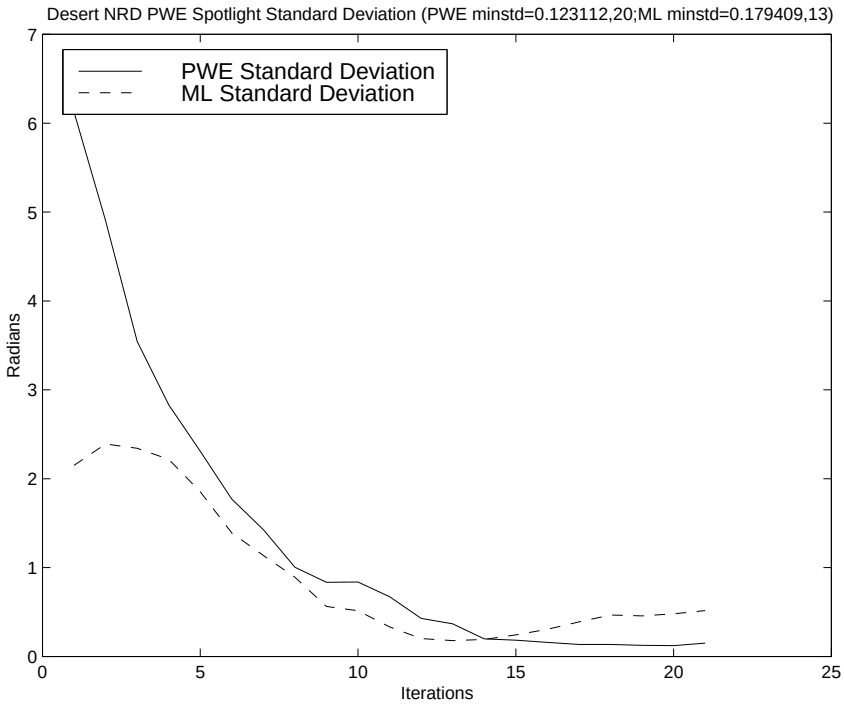

Figure 5: The standard deviation as a function of iteration for PWE-PGA and ML-PGA, non-range dependent spotlight desert image.

similarities with the standard spotlight azimuth compression. Note that this algorithm is used only for phase error estimation and not for image formation.

Stripmap Spotlight Compression consists of four steps [5]. The first step is windowing the long stripmap data into smaller sections. This avoids aliasing in later steps and takes advantage of the localized phase history in stripmap data. The second step is multiplication by the conjugate of the azimuth chirp. This corresponds to the dechirping usually done in hardware on spotlight mode systems. The third step is Fourier transformation, which corresponds to spotlight mode azimuth compression. The final step is applying the stripmap PGA algorithm. This is similar to the spotlight version except that special care must be taken in the circular shifting step. The mean phase gradient is also removed to insure a smooth integration across section boundaries. Any PGA phase estimator may be used in this step, including range dependent or non-range dependent versions.

This method has been shown to work on simulated data. Range-compressed stripmap data is simulated from an actual SAR image by convolving with an azimuth chirp. Then phase errors are applied and estimated using the SSC method. Parameters similar to those for YSAR were used in these simulations. Results were comparable to spotlight mode PGA for the same phase errors applied to the same images.

CONCLUSIONS AND FUTURE WORK

The PGA algorithm has been widely used in spotlight SAR images to remove motion-induced blur. PGA has been proven to be a robust, computationally superior autofocus algorithm. The conventional PGA uses a narrow beam approximation to avoid range dependencies. We have introduced a new phase estimator for use in PGA and have extended it to the range-dependent case. We have also introduced a new algorithm for spotlight compression of stripmap mode SAR data for phase estimation. Several tests have shown that these algorithms can be successful at removing range-dependent and non-range dependent phase errors.

There is still much work to be done on this topic. It was noted that the PWE-PGA converged more slowly than ML-PGA. We may be able to minimize or eliminate this effect through better choice of window size or other parameters. The SSC method will be applied to real YSAR data. This algorithm will also be analyzed to determine the effects of the section boundaries on the phase estimate.

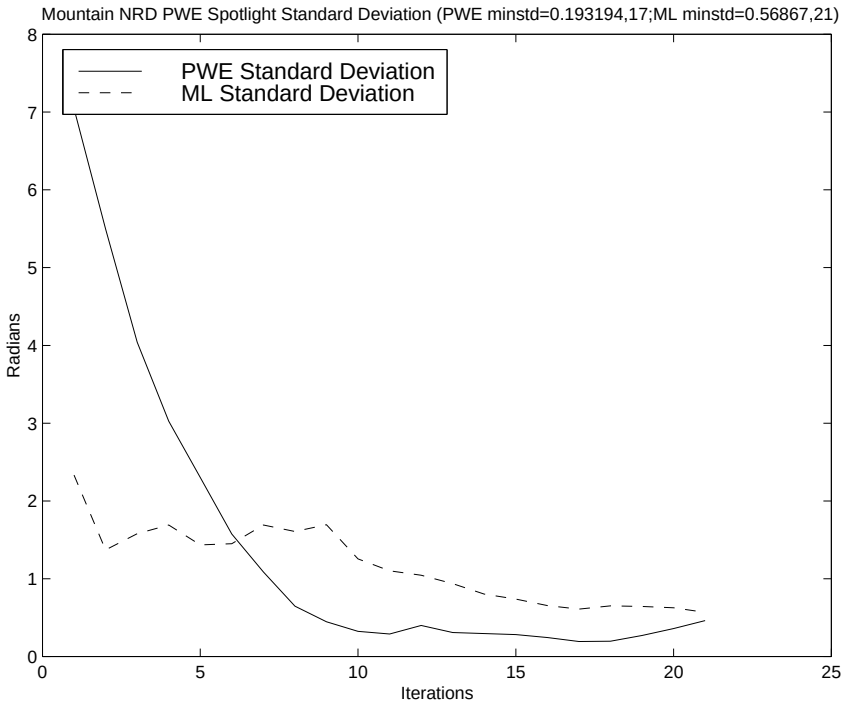

Figure 6: The standard deviation as a function of iteration for PWE-PGA and ML-PGA, non-range dependent spotlight mountain image.

ACKNOWLEDGMENTS

This work was supported in part by a National Science Foundation Graduate Research Fellowship to DGT.

*

References

[1] D. G. Thompson, D. V. Arnold, D. G. Long, G. F. Miner, and T. W. Karlinsey. Ysar: A compact, low-cost synthetic aperture radar. In *Proceedings of the 1996 International Geoscience and Remote Sensing Symposium*, pages 1892–1894, Lincoln, Nebraska, May 1996.

[2] P. H. Eichel and C. V. Jakowatz Jr. Phase-gradient algorithm as an optimal estimator of the phase derivative. *Optics Letters*, 14(20):1101–1103, October 1989.

[3] Charles V. Jakowatz Jr. and Daniel E. Wahl. Eigenvector method for maximum-likelihood estimation of phase errors in synthetic-aperture-radar imagery. *Journal of the Optical Society of America A*, 10(12):2539–2546, December 1993.

[4] D. E. Wahl, P.H. Eichel, D.C. Ghiglia, and C.V. Jakowatz Jr. Phase gradient autofocus - a robust tool for high resolution sar phase correction. *IEEE Transactions on Aerospace and Electronics Systems*, 30(3):827–835, July 1994.

[5] James S. Bates. The phase gradient autofocus algorithm with range dependent stripmap sar. Master's thesis, Brigham Young University, Provo, UT, December 1998.

[6] Y.H. Lu, T.S. Yeo, N.L. Tan, and C.B. Zhang. A stripmap to spotlight data converting algorithm. In *Proceedings of the 1998 International Geoscience and Remote Sensing Symposium*, pages 1168–1170, Seattle, WA, July 1998.

[7] M. Soumekh. Digital spotlighting and coherent subaperture formation for stripmap synthetic aperture radar. *IEEE Transactions on Image Processing*, 21(12):476–480, Dec. 1994.

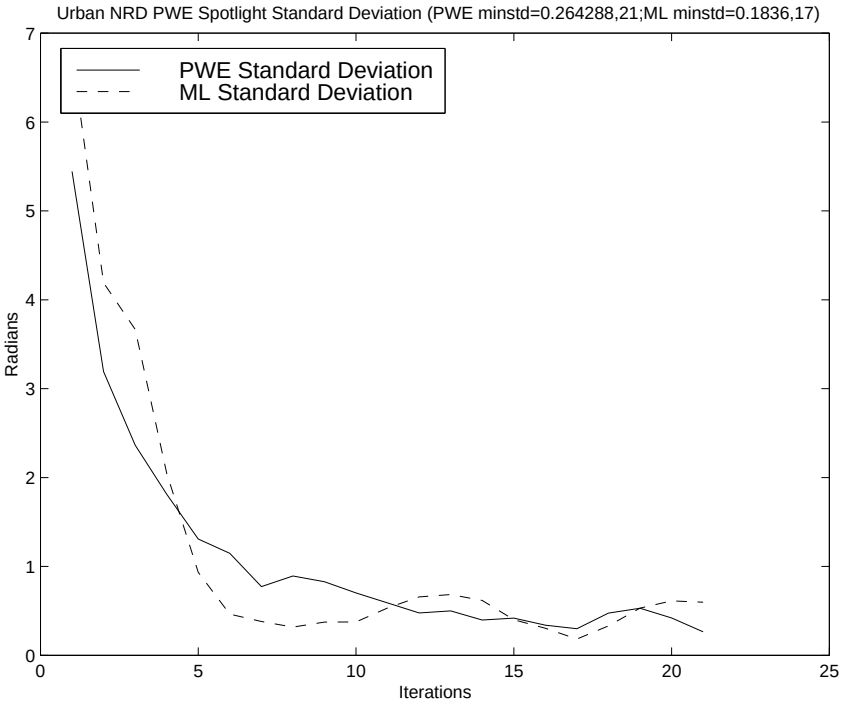

Figure 7: The standard deviation as a function of iteration for PWE-PGA and ML-PGA, non-range dependent spotlight urban image.

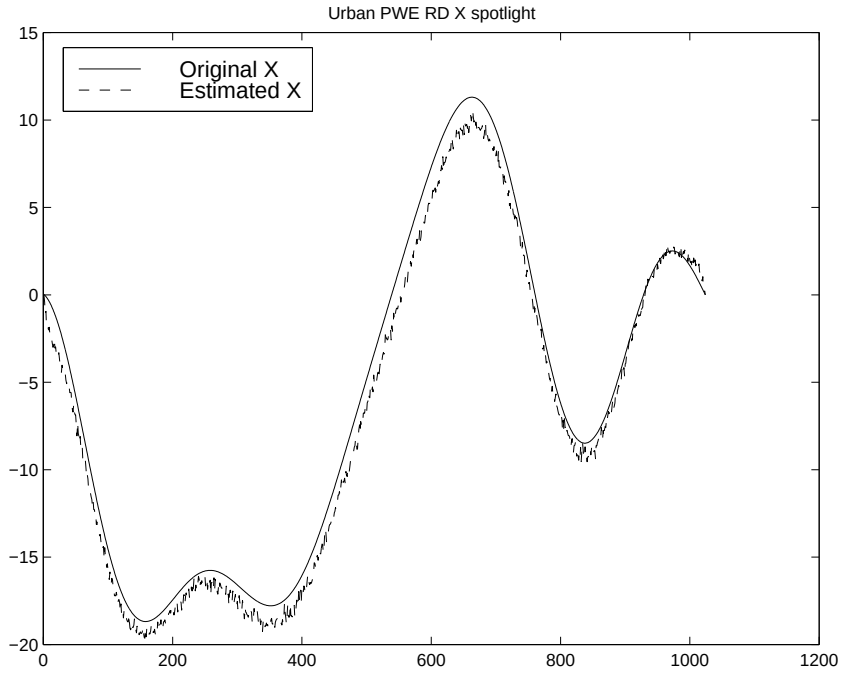

Figure 8: Phase error estimate for ϕ_x, range dependent PWE spotlight urban image.

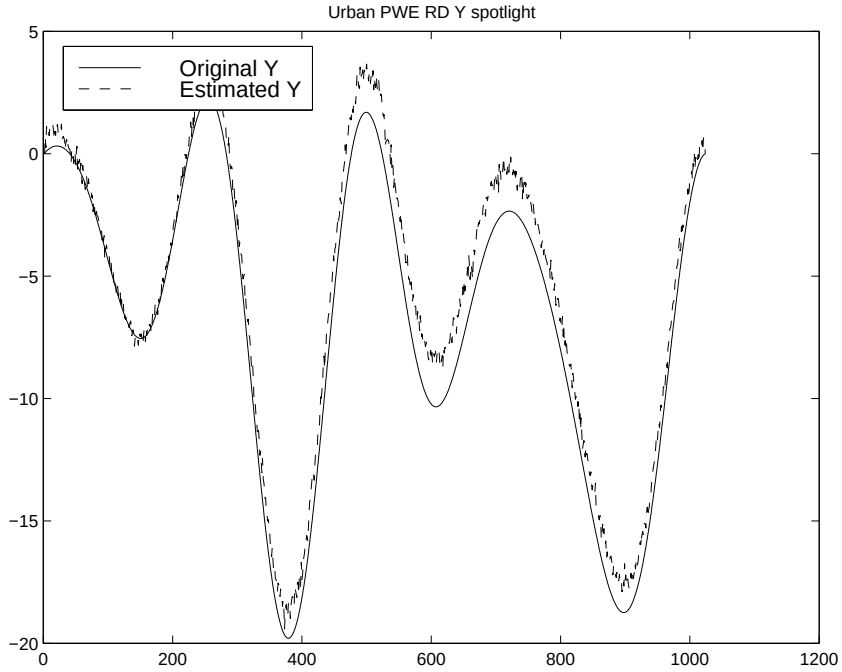

Figure 9: Phase error estimate for ϕ_y, range dependent PWE spotlight urban image.

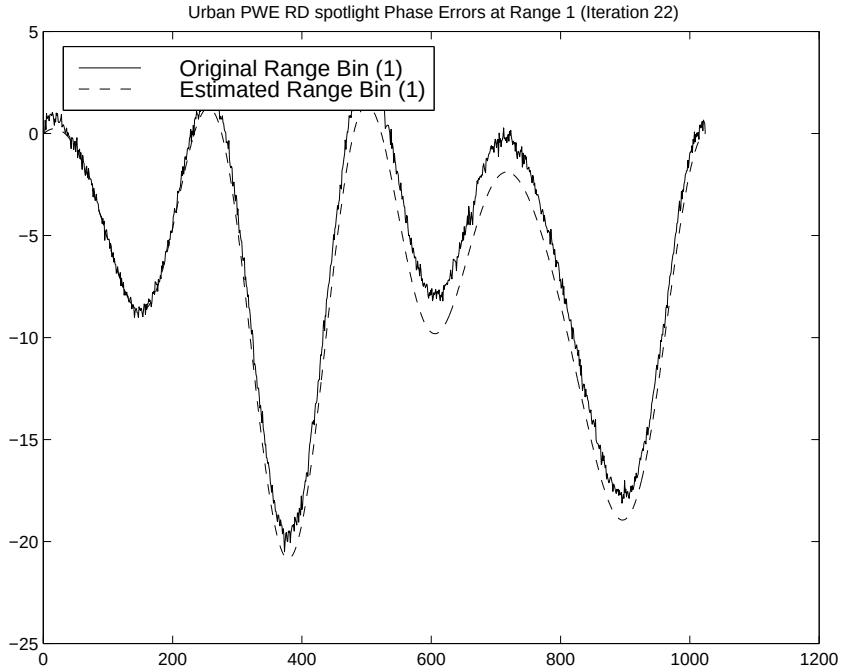

Figure 10: Total phase error estimate for near range, range dependent PWE spotlight urban image. (Range Bin 1)

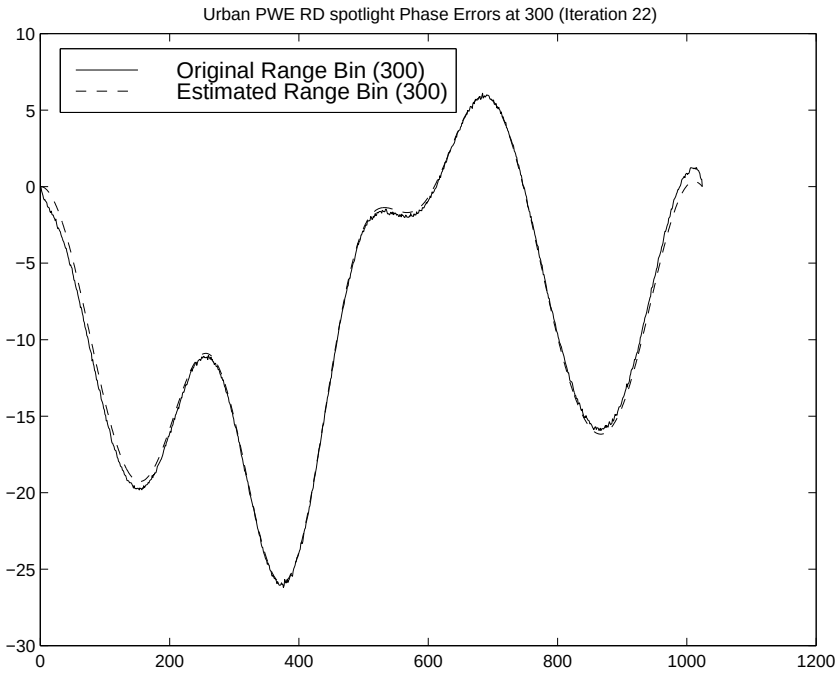

Figure 11: Total phase error estimate for middle range, range dependent PWE spotlight urban image. (Range Bin 300)

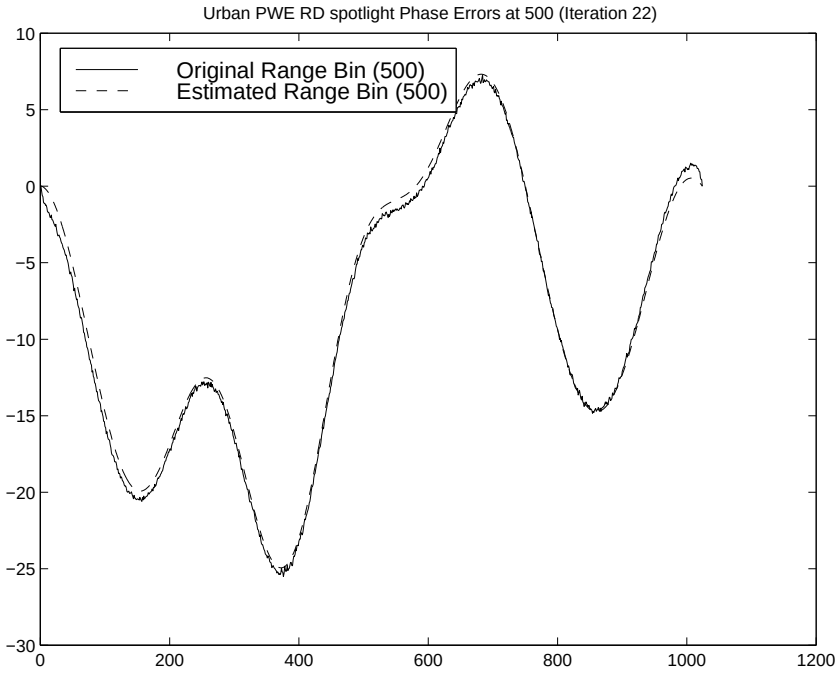

Figure 12: Total phase error estimate for far range, range dependent PWE spotlight urban image. (Range Bin 500)